Desalination and Water Treatment
www.deswater.com

doi: 10.1080/19443994.2015.1084598

57 (2016) 17308–17321
August

Taylor & Francis
Taylor & Francis Group

Preparation of a ceramic membrane from prevalent natural clay for the purification of phosphate wastewater

Baomin Fan[a,*], Gang Wei[b], Hua Hao[c], Anru Guo[d], Jie Li[d]

[a]*Department of Materials Science & Engineering, Beijing Technology and Business University, Beijing 100048, China, Tel./Fax: +86 10 68985337; email: fanbaomin@btbu.edu.cn*
[b]*Beijing Key Laboratory of Electrochemical Process and Technology for Materials, Beijing University of Chemical Technology, Beijing 100029, China, Tel./Fax: +86 10 64454410; email: weig_buct@163.com*
[c]*Institute of Chemistry, Chinese Academy of Sciences, Beijing 100190, China, Tel./Fax: +86 10 82671068; email: haohua@iccas.ac.cn*
[d]*Aerospace Research Institute of Materials & Processing Technology, China Aerospace Science and Technology Corporation, Beijing 100076, China, Tel./Fax: +86 10 68380659; emails: anruguo@126.com (A. Guo), jieli703@126.com (J. Li)*

Received 31 January 2015; Accepted 15 August 2015

ABSTRACT

A ceramic membrane was prepared on SiO_2 support through suspended powder technology from cost-effective natural clay. The sintering temperature was selected at 600°C according to thermogravimetric analysis of the raw powder. Results of Fourier transform infrared spectroscopy and X-ray fluorescence (XRF) showed the natural clay had high physicochemical similarity to phyllosilicate. Crystal structure, pore size distribution, and effective membrane thickness of the natural clay membrane (NCM) were also studied. X-ray diffraction patterns revealed a phase conversion occurs during sintering. The results of mercury porosimetry showed the pore size distribution of NCM ranged from 3 to 10 nm. Scanning electron microscopy images showed NCM distributed uniformly on the support with an approximate thickness of 30 μm. The transport and separation performances of NCM were tested in batch mode through a stirred cell under dead-end mode. It was found that retention of PO_4^{3-} was pH-dependent with the satisfactory rejection rate under alkaline conditions (pH > 10). The analysis of XRF made it reasonable to assume that amphoteric Al_2O_3 in the raw material should be responsible for the effective retention through electrical-related interactions. In addition, both increasing temperature and applying turbulence affected the retention positively. Filtration resistance analysis of treating phosphate solutions indicated that irreversible fouling could be completely neglected, and concentration polarization was the main cause of reversible fouling.

Keywords: Natural clay; Ceramic membrane; Phosphate wastewater; Concentration polarization; Membrane fouling

*Corresponding author.

1. Introduction

Phosphate is considered as an effective water treatment chemical widely used in industrial processes to prevent the essential equipment from corrosion and scaling [1]. For instance, a proper amount of trisodium phosphate (Na_3PO_4, TSP) is usually introduced into the feedwater of power plants to keep boilers running stably and safely. In this regard, significant quantities of phosphate wastewater will be released into the environment. Phosphorus is one of the key nutrient elements that cause eutrophication in aquatic eco-systems: superfluous phosphate discharged into natural water bodies often leads to the depletion of dissolved oxygen and overgrowth of algal [2]. In addition, discharging wastewater with high temperature can cause a huge energy waste [3]. Therefore, based on both environmental and economic points of view, it is of value to recover phosphate wastewater to generate sufficient make-up water for industrial purpose.

Research efforts are under way to address the problem of phosphate pollution: advanced treatments of phosphate wastewater have been achieved by adsorption, chemical precipitation, membrane technology with different degrees of success [4–6]. In recent years, membrane technologies have gained increasing attention due to their potential application in a wide range of industrial processes and pollution control [7–9]. In addition, membrane processes hardly transform pollutants or re-contaminate the treated water. Several papers on the treatment of phosphate wastewater have been available within last three years. For example, ion-exchange membranes based on polymer were arranged under an electrical field by Tran and co-workers for concentration of phosphate from wastewater through selectrodialysis [10]. Shang et al. [11] found that dissolved phosphate could be effectively rejected by tight TiO_2 membrane through electrostatic interactions.

Organic membranes, usually made of various polymers, are materials commonly used for the treatment of drinking, process and wastewater streams; however, they possess some performance limitations when compared with those inorganic counterparts: ceramic membranes are generally more chemically and thermally resistant than polymeric ones [12–14]. These intrinsic properties are of great concern in the aggressive cleaning and operation of membrane for ceramic membranes, as they hardly suffer the "membrane/pore swelling effect" or degradation when exposed to oxidants, strong acids or bases, and high temperatures [8,11,15]. Given that temperature of industrial effluents is usually high (over 40˚C), it is not conducive for polymeric membranes to keep high separation efficiency and long guarantee period [16]. Therefore, ceramic membranes appear to be attractive for treating wastewater with high temperature due to its high efficiency, stability, and operability.

Ceramic membranes, especially based on alumina and silica, have confirmed that they obtained long operating life, chemical inertia, and thermal stability [17]. It is also generally known that there are rich deposits of silicon and aluminum in the continental crust, and membranes containing alumina often exhibit amphoteric characteristics, which is prone to establish electrical-related interaction with ionic pollutants. Therefore, some natural materials can be used as found or after appropriate transformations for membrane fabrication. Currently, significant efforts have been devoted to the preparation of ceramic membranes mainly made from Al_2O_3, TiO_2, and ZrO_2 through sol–gel method [18–20]. In addition, most previous research focused on separating the relatively large polluting agents, such as natural organic matter, textile effluents, and oil/water system [21,22]. However, eliminating ions by ceramic membrane made from natural minerals has not hitherto been studied.

This present work seeks to prepare a natural clay membrane (NCM) on the commercial SiO_2 support by dip-coating method, with a special attention on the purifying capacity of wastewater containing phosphate. The as-prepared membrane shows a mean pore size that can be classified into the tight ultrafiltration category, which is also a charged membrane by electrokinetic characterization. Through dead-end filtration mode, the separation efficiency of phosphate, influence factors of filtration, and membrane fouling are discussed.

2. Materials and methods

2.1. Chemicals

Natural rocks were sampled from local mountain of Suzhou region (Jiangsu, China), which was crushed into large particles, ground into powder, and sieved by a 140 mesh sieve to obtain the natural clay powder. The particle size distribution of raw powder was determined through a Mastersizer 3,000 style laser particle size analyzer (Malvern, Britain), which was ranging from 4 to 97 μm.

Analytical grade Na_3PO_4, sodium hexametaphosphate (SHMP), HCl, HNO_3, and NaOH were obtained from Beijing Chemical Works and used as received. All the solutions mentioned in this study were prepared using deionized (DI) water with the conductivity of 7.8 μS/cm, which was prepared through a HA-10LB style ultra-pure water system (Berclean

Company, Chongqing) and used at its native pH (6.0 ± 0.2). Commercially available SiO_2 supports (Fengxi Porcelain Factory, Chaozhou) were used as the flat disc type. Technical parameters of the support applied in the measurements are listed in Table 1.

2.2. Preparation of NCM

Initially, pre-treatment of SiO_2 supports were carried out, by grinding with emery paper of 1,000–2,000 grit, rinsing with DI water, ultrasonic cleaning in dilute nitric acid (pH 3), and dried at ambient temperature (AT, ~26˚C) before the coating procedure.

The natural clay powder (6.5 wt.%) was mixed with DI water with a proper amount of SHMP as the dispersant to obtain a deflocculated suspension, which was kept in a Petri dish. One side of the SiO_2 support was dipped in the suspension for 10 s and a coating layer could be formed. The coated supports were placed in a desiccator over silica gel at AT for 24 h. After natural drying, coated supports were oven-dried at 90˚C to remove residual moisture, and then sintered at 600˚C for 2 h with a heating rate of 1˚C/min in a SX2–2.5–12 style muffle furnace (Beijing Furnace Factory, China). Each as-prepared membrane was carefully collected before characterizations and performance tests.

2.3. Static characterization of NCM

The chemical compositions of natural clay were analyzed by a XRF-1,800 XRF spectrometer (XRF, Shimadzu).Thermal gravimetric analysis (TGA) was performed on a TA Q50 thermogravimetric system at a heating rate of 10˚C/min under air atmosphere with a flow rate of 60 cm^3/min. The surface morphology was observed through a HITACHI S-4,700 style field emission scanning electron microscope (SEM). The crystal structures of raw powder and as-prepared membrane were studied by X-ray diffraction (XRD; D/max2500VB 2+/PCX, Rigaku) using CuKα radiation with 2θ from 5˚ to 90˚. FTIR spectra of the samples were finished using a Nicolet 6,700 spectrometer between 4,000 and 400 cm^{-1}; the samples were prepared in the pellet form using spectroscopic grade KBr powder. The pore size distribution was obtained from a Micromeritics AutoPore IV9500 mercury porosimeter. Zeta potential of the membrane was obtained through streaming potential analysis with Helmholtz-Smoluchowski model [23]; the desired pH values were adjusted by dilute NaOH and HCl solutions and monitored by a pH meter (PHS-3C, Shanghai Leici). The contact angle was measured through a Dataphysics OCA 20 optical contact angle system by the sessile drop method [24].

Table 1
Parameters of the commercial SiO_2 support

Parameter	Value
Configuration	Flat disc
Diameter (mm)	60
Thickness (mm)	3.80
Porosity (%)	30.34
Compression strength (MPa)	17.58

2.4. Dynamic characterization of NCM

The test solutions were prepared by dissolving a known weight of TSP in DI water under stirring to give the desired concentration. All samples were prepared in triplicate.

Experiments were carried out through a lab-made stirred cell with a volume of 400 mL as depicted in Fig. 1. A thin layer of porous steel was placed between the membrane and permeate outlet to avoid any deviation of results caused by the rough permeate channel surface. A magnetic stirrer on the top of the cell would rotate the agitator blade, which was connected to a control chamber for speed adjustment. The testing temperature was controlled by a thermocouple fixed in the cell. All filtrations were run in duplicate or more to check the reproducibility.

In order to minimize any structural change of the prepared membrane, a compaction procedure was conducted as follows: the fresh membrane was immersed in DI water for at least 2 h and then was conditioned through filtering DI water under

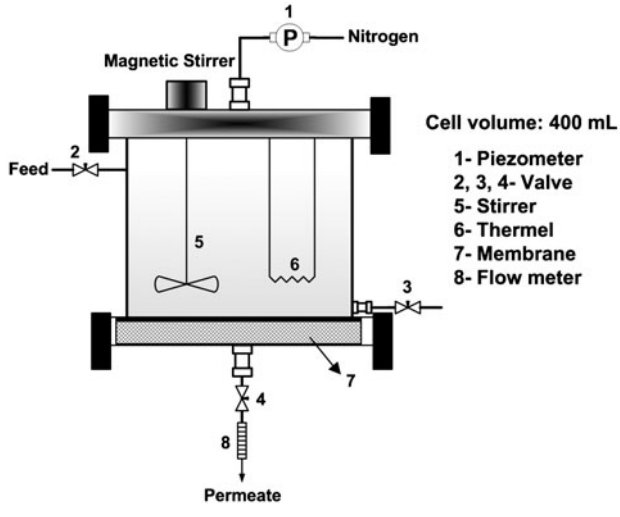

Fig. 1. Schematic diagram of the stirred cell.

0.6 MPa for 1 h. The membrane was also allowed to equilibrate in the test solution for a while before each experimental run.

Water flux was measured as the cumulative mass of permeate, which was recorded during filtration over an electronic balance connected to a computer. The hydraulic permeability (L_p) was assessed from the water fluxes under driving pressures (ΔP) varying from 0.10 to 0.38 MPa. Retention of phosphate was determined by taking samples of permeate and feed under steady state at 0.15 MPa. Concentration of phosphate in the sample was determined by the molybdenum blue colorimetric method [25], and the rejection rate (η, %) was calculated according to the following equation:

$$\eta = (1 - C_p/C_f) \times 100\% \quad (1)$$

where C_p and C_f represent phosphate concentrations in the permeate and feed, respectively, mg/L.

2.5. Resistance analysis

The measurement of filtration resistances based on flux data could provide additional insight on the process of membrane separation. According to constant pressure theory and Darcy's law [17,22], the total filtration resistance (R_t, m^{-1}) has a relationship with permeate flux (J, m/s):

$$J = \Delta P/(\mu \cdot R_t) \quad (2)$$

where ΔP is the driving pressure, Pa; and μ is the dynamic viscosity of the feed, Pa·s.

According to resistance-in-series model, the total resistance is often divided into several components depending on the situations in detail [7,22,26]. Regarding the specific conditions of this study, R_t should be comprised of three main subdivisions: intrinsic membrane resistance, R_m, adsorption resistance, R_{ads}, and fouling resistance, R_f. In addition, the fouling resistance can be further subdivided into two parts: reversible fouling resistance, R_{rev}, and irreversible fouling resistance, R_{irr}. It is of value to mention that adsorption resistance results from weak physical intermolecular forces between membrane and contaminants, which is thermodynamically unavoidable; whereas, in dead-end mode, reversible fouling is mainly caused by the concentration polarization, which can be targeted by physical cleaning or mild chemical cleaning; however, irreversible fouling cannot be eliminated using chemical cleaning. In summary, the following equations can be established.

$$R_t = R_m + R_{ads} + R_f \quad (3)$$

$$R_f = R_{rev} + R_{irr} \quad (4)$$

Each type of resistance was obtained by designing a series of filtration experiments and measuring the flux at the end of each step under given conditions. The analysis protocol to determine resistances is listed in Table 2.

On account of the flux data, various hydraulic resistances could be calculated using Hagen-Poiseuille equation [27]:

$$J_{w1} = \frac{\Delta P}{\mu_w \cdot R_m} \quad (5)$$

$$J_{w2} = \frac{\Delta P}{\mu_w \cdot (R_m + R_{ads})} \quad (6)$$

$$J_{w3} = \frac{\Delta P}{\mu_{pw} \cdot (R_m + R_{ads} + R_f)} \quad (7)$$

$$J_{w4} = \frac{\Delta P}{\mu_w \cdot (R_m + R_{irr})} \quad (8)$$

where μ_w and μ_{pw} are the dynamic viscosity of DI water and 200 mg/L TSP solution, respectively, Pa·s. At room temperature (~26°C), μ_w equals 0.8737 mPa·s and μ_{pw} equals 0.9218 mPa·s [28].

3. Results and discussion

3.1. Characterization of the natural clay

The chemical compositions could determine the properties of ceramic materials to some extent. The elemental analysis of the natural clay was performed by XRF technique with the results given in Table 2. The major composition found in the sample is SiO_2 (58.91 wt.%) similar to the material of support, which can positively affect the adhesion force between the support and active layer during sintering [3]. In addition, the clay contains relatively high concentration of Al_2O_3 (35.32 wt.%), which shows the amphoteric characteristic controlled by pH [19]. Therefore, the membrane obtained from natural clay might exhibit permselectivity caused by electrical-related effects for electrolyte solutions, which will be discussed in the following text.

In order to determine the optimal temperature for membrane forming, the thermal property of raw clay is studied through TGA presented in Fig. 2. It is worth mentioning that the thermal analysis was conducted

Table 2
The analysis protocol for wastewater treatment

Procedure	Operation	Parameter
Pure water flux	The pure water flux of a fresh membrane was determined	J_{w1}
Adsorption test	A fresh membrane was immersed in a solution containing 200 mg/L TSP for 3 h, and then the pure water flux was determined	J_{w2}
Fouling test	After repeating the adsorption test, filtration of phosphate solutions (200 mg/L TSP) was conducted	J_{w3}
Flushing	Subsequent to the fouling tests, the membrane was subject to the backwashing procedure under 0.3 MPa using DI water, followed by a pure water flux determination	J_{w4}

under air environment; thus, the practical thermal behavior of natural clay in the preparation process could be monitored. Analysis of TG curve shows that the major weight loss occurs before 69.16˚C, which is due to the removal of weakly absorbed water. However, an increment of weight starts at 151.18˚C, which might result from the reaction between metallic oxides in the clay and CO_2 from the environment. Then, the weight keeps relative stable with the elevated temperature until approx. 573˚C. Owing to the phase transformation from β-quartz to α-quartz, a small peak appears at 593.65˚C [29]. An appreciable pyrolysis stage starts at 654.33˚C mainly attributes to the volatilization or decomposition of some compositions in the raw material; thus, the intrinsic structure might be destroyed along with the losing of certain properties.

Moreover, alumina kept in the clay plays a key role in the formation of the membrane. Schaep and coworkers [30] have revealed that increasing temperature would be accompanied by pore enlargement of

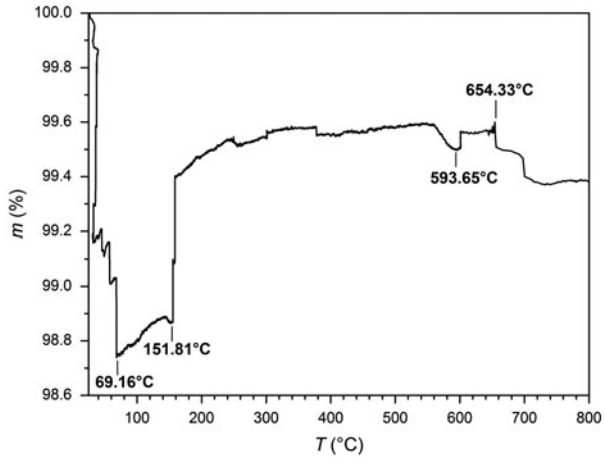

Fig. 2. TGA curve of the natural clay.

Al_2O_3 membranes. Combined with the thermal analysis, the sintering temperature for a defect-free NCM should not exceed 654.33˚C. On the other side, the sintering temperature should be higher than 573˚C preferably, at which the phase transformation occurs. It is noteworthy that α-quartz can be re-transferred to β-quartz during environmental cooling. This reversible phase conversion between α- and β-quartz is propitious to eliminate the residual stress among adjacent lattices [29]. Therefore, the sintering temperature for NCM was selected at 600˚C in our investigation.

3.2. Membrane properties

Fig. 3(a) and (b) show the results of mercury porosimetry for SiO_2 support and the supported NCM, respectively. It is worth mentioning that the active layer cannot be totally detached from support; therefore, the determination of pore size distribution for NCM, materially, includes the pore size distribution of both active layer and SiO_2 support. According to Fig. 3(a), the most concentrative pore diameter of SiO_2 support ranges from 400 to 1,000 nm indicating a macroporous category. Fig. 3(b) shows that two peaks appear in the curve: a sharp peak centered at 1,000 nm corresponds to the pores of SiO_2 support, and a broad peak ranging from 3 to 100 nm corresponds to the pores of active layer. Another aspect deserves attention that the cumulative pore area increases sharply since the pores with 12 nm width based on Fig. 3(b), which indicates the main distribution of majority pores for active layer. Additional insights on Fig. 3(a) and (b) reveal that the cumulative pore area of NCM is obviously higher than those of SiO_2 support, which can be assigned to the complex networks of interconnected pores in the active layer [31].

SEM images shown in Fig. 4 show the morphology of support, active layer, and cross-section of NCM.

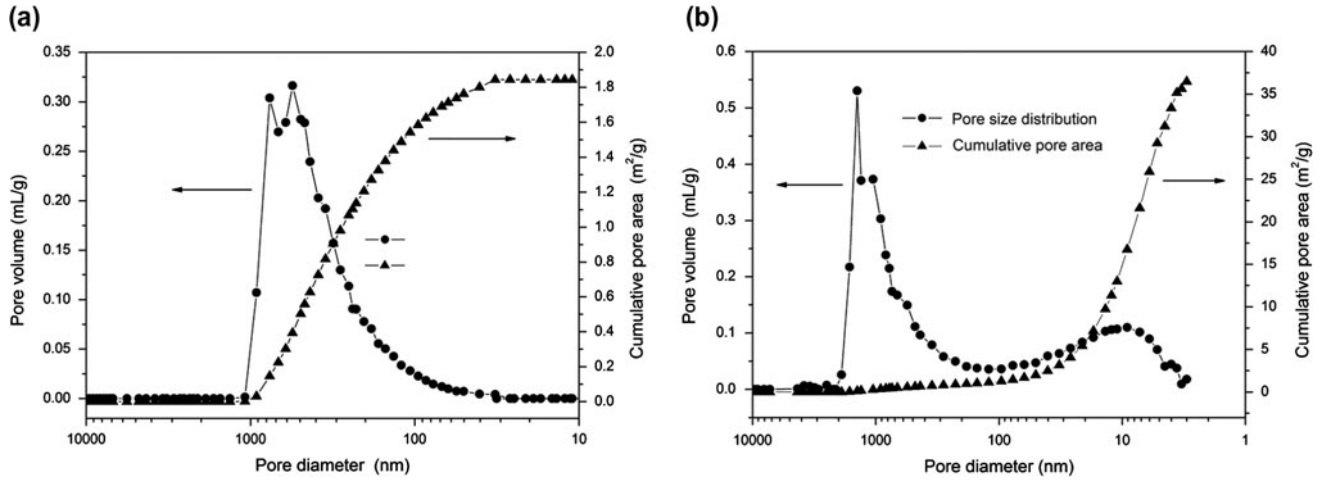

Fig. 3. Results of mercury porosimetry for (a) SiO_2 support and (b) the supported NCM.

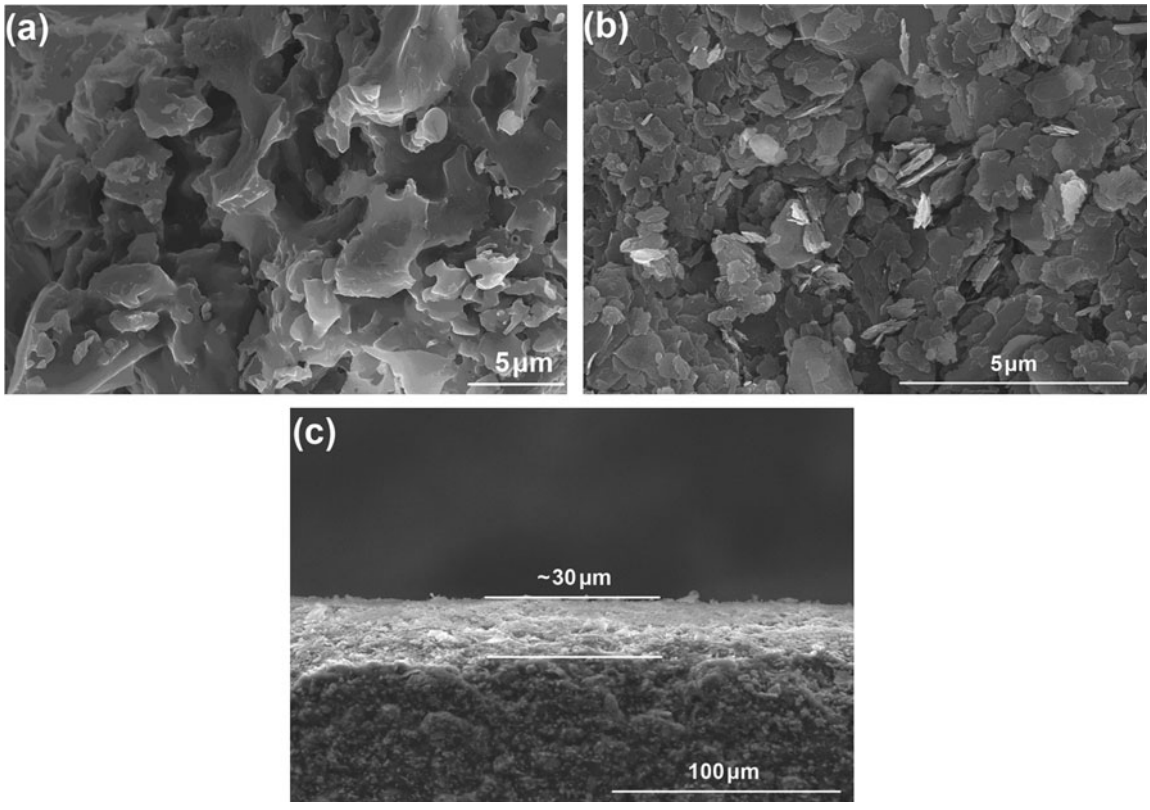

Fig. 4. SEM images of (a) SiO_2 support, (b) active layer, and (c) cross section of the sample.

Fig. 4(a) and (b) provide the indirect evidence in support of the conclusion of pore size distribution drawn earlier. In addition, comparison of Fig. 4(a) and (b) discloses that the active layer possesses a more compact surface than support does. It is of value to mention that the particles of natural clay present an appearance of flat sheet, which would hardly intrude into the pores of support during the dip-coating process in contrast to that of fine spherical particles. Thereby, it is unnecessary to prepare the traditional intermediate layer for a high-performance membrane. Irregular accumulation of sheet particles is also

conducive to obtain a layer with high porosity and tortuosity. According to Fig. 4(c), the top layer can be clearly distinguished from the support with an approximate thickness of 30 μm from a cross-sectional view.

XRD analysis (Fig. 5) allows specifying the crystal changes for natural clay after sintering. The pattern of SiO_2 support shown in Fig. 5(a) keeps the original shape after sintering, indicating the stability during membrane forming. Quartz is the main constituent of the support, which is in line with other reports [32]. Fig. 5(b) exhibits a series of intense sharp peaks indicating the main crystalline phases of natural clay: kaolinite, muscovite, and quartz. Compared with the diffractogram of unsintered powder, the peak corresponding to kaolinite phase is disappeared in the crushed powder of active layer according to Fig. 5(c). Zhou et al. [33] have attributed this phenomenon to the phase conversion at a temperature over 500˚C, which could be described in following equation.

$$\text{Kaolinite} \xrightarrow{\text{over } 500^{\circ}\text{C}} \text{metakaolinite} + H_2O \quad (9)$$

Moreover, this phase conversion at the desired temperature (600˚C) is prone to rearrange crystalline phases, followed by stabilizing the internal structure of active layer.

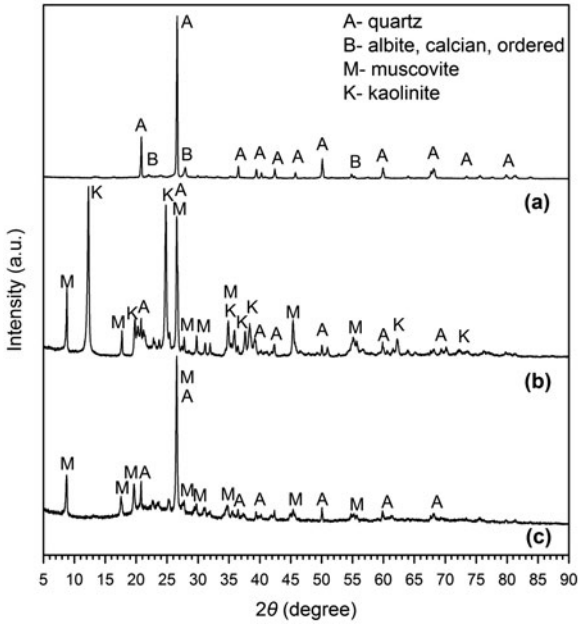

Fig. 5. XRD patterns of (a) SiO_2 support, (b) natural (c) clay, and crushed membrane powder.

FTIR spectra of the natural clay and crushed powder of active layer are shown in Fig. 6, and the assignment of the main vibration bands, based on previous studies [34–37], is listed in Table 3. According to Fig. 6, the spectrum of natural clay after sintering still keeps the characteristic peaks assigned to O-H stretching and bending vibration. For this reason, it is rational to assume that the natural clay used in our study can be classified as the phyllosilicate, which contains quantities of inner hydroxyl groups in the structural unit layer [14,38]. On the other hand, the deformation vibration of Al-O-Al in the fingerprint region are better outlined, as compared to the raw powder. This is the result of a better structural ordering in NCM leading to the enhanced surface charge performance [20,39] (Table 4).

3.3. Permeability and separation performance

Initially, NCM is characterized by water permeability depicted in Fig. 7. For each fresh membrane, flux increases with the elevated driving pressure over the range studied. It can be observed from Fig. 7(a) that all the fluxes are stabilized in about 5 min. In addition, water flux is directly proportional to the applied pressure according to Fig. 7(b). The slope of the line in Fig. 7(b) corresponds to the membrane intrinsic permeability (L_p) according to Darcy's law [21], which is 1456.38 L/(m^2 h MPa) after calculating. It is noteworthy that permeability of NCM is smaller than that of reported values with the similar pore size distribution [12,17,22]. The relative low permeability can be due probably to the high thickness of top layer as presented in Fig. 4(c).

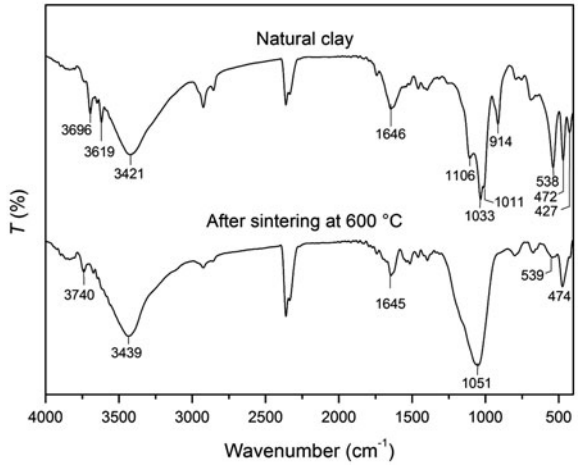

Fig. 6. FTIR spectra of the natural clay and crushed membrane powder.

Table 3
The chemical compositions of natural clay. LOI is loss on ignition

	The chemical composition (wt.%)									
Material	SiO_2	Al_2O_3	K_2O	Fe_2O_3	MgO	TiO_2	SO_3	P_2O_5	MnO	LOI
Natural clay	58.91	35.32	3.44	1.33	0.41	0.31	0.10	0.05	0.02	0.11

Table 4
Assignment of the main vibration bands of natural clay and crushed membrane powder

Main vibration bands(cm^{-1})		
Natural clay	After sintering	Assignment
3,696, 3,619, 3,421	3,740, 3,438	ν_{as}(–OH/inner hydroxyl) hydrogen bond with O–Si
1,646	1,645	γ_{as} (inner hydroxyl)
1,106, 472, 427	474	δ(Si–O–Si)
1,033	1,051	ν(Al–O–Al) octahedral
1,011, 538	539	δ(Si–O–Al) octahedral
914	–	δ(AlO–H)

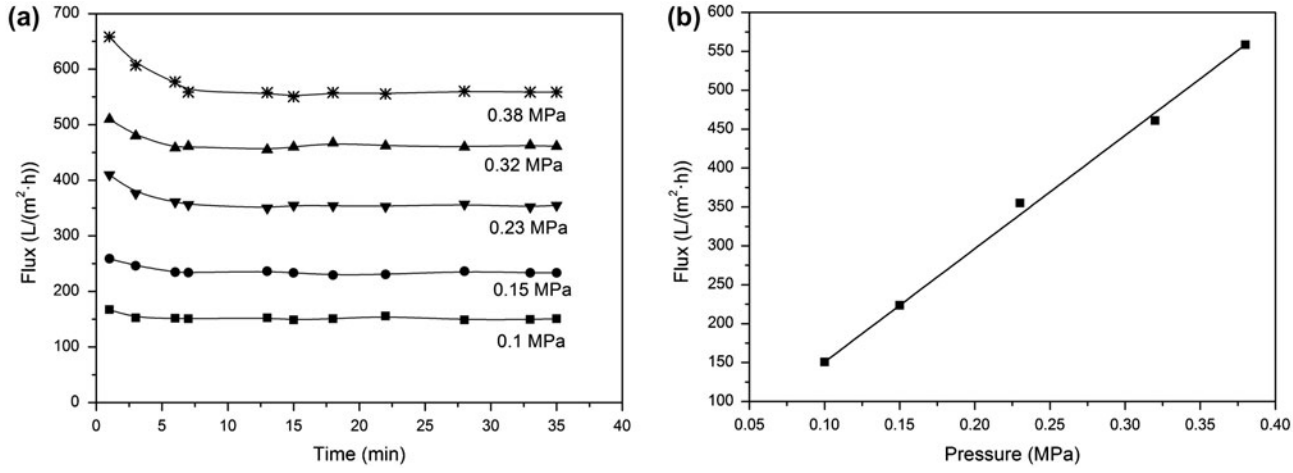

Fig. 7. Variation of pure water flux as (a) a function of working time and (b) pressure at 26°C.

Fig. 8 illustrates the evolution of the permeate flux of NCM at various TSP concentrations under 0.15 MPa. In order to minimize deviations owing to nuances of different experimental individuals, normalized flux (J_r) is used as the ratio of permeate flux (J_p) to the initial flux at the beginning of the filtration (J_w). It can be observed that, in general, normalized flux decreases with time for each concentration level, which commonly results from the solutes driven towards the membrane surface and deposited thereafter [40]. Moreover, all the fluxes of NCM for TSP solutions are lower than that in the control group (DI water). This may be attributed to the presence of Na^+ in TSP solutions, which can adversely affect the flux [41]. Besides, electroviscous effect caused by phosphate in the narrow pores of feed side may also deteriorate the flux with the increasing TSP concentration [42].

Closer inspection of Fig. 8 reveals that the flux exhibits the increasing trend with the elevated concentration of TSP until 150 mg/L. According to the conclusion drawn by Lee and Kim [26], increasing

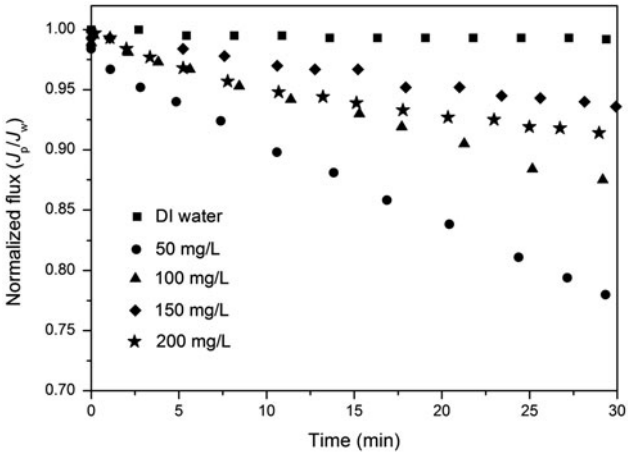

Fig. 8. Effect of TSP concentrations on normalized flux under 26˚C.

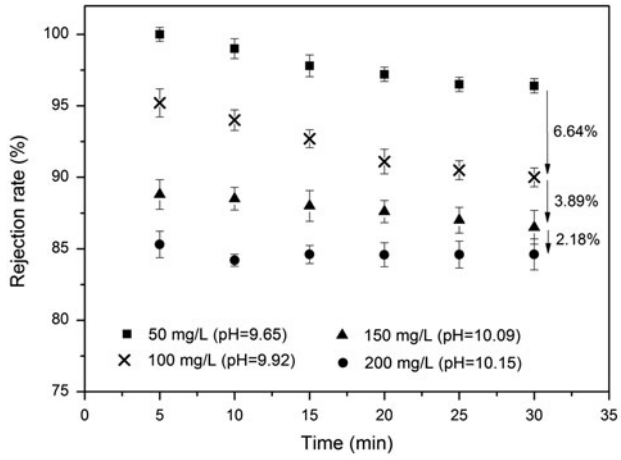

Fig. 9. Retention of TSP by NCM at 26˚C under constant pressure of 0.15 MPa.

alkalinity or salt content of the feed is propitious to obtain high flux. For this regard, increasing the concentration of TSP cannot only increase the alkalinity, but also raise the salt content. Therefore, the flux increases monotonously over the concentration range from 50 to 150 mg/L. However, the flux for 200 mg/L TSP solution is lower than that for the solution containing 150 mg/L TSP. As essays progress, it is always assumed that the concentration polarization in filtration process will reduce the effective driving pressure, followed by the decreased flux [7,26]. Thus, excessively high concentration of TSP in the feed creates a thick polarization layer, which largely suppresses the permeate flux. It is necessary to elucidate that concentration polarization occurs in each tested solution (50, 100, and 150 mg/L) as well, but not be so pronounced as that of 200 mg/L TSP sample.

In summary, raising the concentration of TSP can increase the alkalinity of solution, which is conducive to obtain high flux. However, high concentration of TSP can produce noticeable concentration polarization phenomenon during filtration. Therefore, an antagonistic effect between alkalinity and concentration polarization is obvious.

The retention data as a function of TSP concentration are given in Fig. 9. An essential conclusion can be drawn that NCM is effective for purifying phosphate wastewater: the rejection rate of TSP can be still satisfactory (~85%) even at 200 mg/L of salt concentration. With the pore size distribution of NCM shown in Fig. 3(b), it is apparent that steric exclusion will be of no importance in the case of inorganic ions, which could be only rejected by charge effects [43]. Therefore, characteristics of ions rejection and permeate flux can be attributed to the surface electrical properties of NCM. Combined with the results of XRF (Table 2) and FTIR (Fig. 6), aluminum oxide, which is an amphoteric material contained in the natural clay, may play a key role in the rejection process.

It is worth further attention on Fig. 9 that the rejection rate shows the decreasing trend for each concentration level with operating time. There is a distinguishable initial decrease of permeate flux due to adsorption, pore blockage, concentration polarization, or formation of fouling layer within 15 min operation, after which the permeate flux reaches a relative steady-state. For another aspect, the rejection rate decreases as the pH of feed solution increases with the increasing TSP concentration. This pH dependency needs additional characterizations, which is shown in Fig. 10, for harvesting the insight on retention mechanism.

Fig. 10(a) shows that the retention curve exhibits a highly asymmetric S-shape, which is the signature of amphoteric membranes in rejecting asymmetric electrolyte (TSP) principally by electrostatic interactions. In other words, the salt retention is dominated by ions with high valence (PO_4^{3-}) because they hold more charges [8]. In the low pH range (less than 6), the active layer of NCM is positively charged, which is evidenced by zeta potential shown in Fig. 10(b). Thus, the surface of NCM favorably interacts with negatively charged species (HPO_4^{2-}, $H_2PO_4^-$); as a result, a large amount of counter-ions will aggregate on the surface or in the pores, and eventually diffuse across the membrane yielding a low rejection rate. As the pH increases (over 6), retention increases because NCM changes to be negatively charged. On this occasion, more and more anions are repelled by NCM for the increase of negative charge. In addition, it is accepted

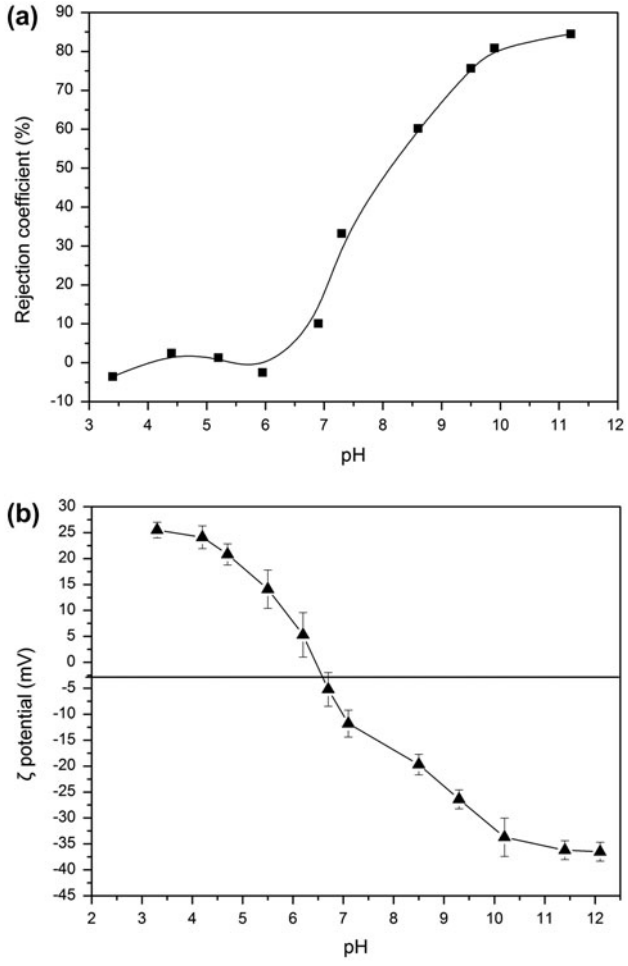

Fig. 10. (a) Retention of TSP asa function of pH at fixed concentration of 200 mg/L and (b) zeta potential of NCM in presence of the indifferent electrolyte: NaCl with equal ionic strength of TSP.

that NCM exhibits the electrical property with an isoelectric point (IEP) at pH around 6.4 based on Fig. 10(a) and (b).

Furthermore, another aspect still deserves attention that a negative retention is obtained before IEP shown in Fig. 10(a). For dead-end mode, concentration polarization leads to an excess of counter-ions gathered near the surface of charged membrane. As a result, the concentration of TSP near the surface (both the feed and permeate side) can be higher than that in bulk solution. Therefore, it is possible to obtain a negative retention when the net charge of NCM is relative low. Mazzoni et al. [44] have already reported the similar results.

Subsequent to clarify the amphoteric nature of NCM, some interpretations can be put forward to elucidate the difference of separation performances with various TSP concentrations shown in Fig. 9. It can be observed that the pH value of each concentration is higher than IEP of NCM, so that the membrane is negatively charged once contacting the solutions. However, with increasing concentration, more diffusion of co-ions (PO_4^{3-}) can take place as a consequence of a higher driving force resulted from concentration difference, so that a decrease in retention is observed. In addition, screen effect caused by counter-ions (Na^+) will be pronounced with the elevated concentration leading to a decrease of repulsive force between membrane and co-ions.

With respect to the retention of TSP, it also should be remarked that, as more TSP is added, retention further declines but to a less extent. As the concentration of TSP increases from 50 to 100 mg/L, from 100 to 150 mg/L and from 150 to 200 mg/L, the rejection rate at the end of filtration decreases by 6.64, 3.89, and 2.18%, respectively. The reason for this phenomenon is somewhat complicated, because both flux and salt concentration play the crucial role. On one hand, dilution effect appears due to the increase of flux as shown in Fig. 8, which can lower the ions concentration in the filtrate [45]. On the other hand, increasing feed concentration leads to the enhanced electroviscous effect in membrane pores, which can retard the diffusion of solutes from bulk solution to permeate side, consequently, lower the decrement of rejection rate [42].

3.4. Fouling analysis

The determination of filtration resistances from flux data can provide additional insight on the fouling mechanism. The various resistances components are summarized in Fig. 11, noting that the analysis protocol is previously mentioned in Section 2.5. As it can be observed, the intrinsic resistance (R_m), which is related to only membrane properties, is considered to be a constant value of 2.78×10^{12} m^{-1} and dominates through the filtration. The resistance derived from adsorption (R_{ads}, 0.63×10^{11} m^{-1}) also remains nearly stable implying that adsorption takes place first once membrane and solutes are in contact. With regard to the fouling resistance (R_f), including reversible (R_{rev}) resistance with its irreversible (R_{irr}) counterpart, it maintains increasing tendency with time owing to the increase of R_{rev}. The increasing R_{rev} can be assigned to concentration polarization, which deteriorates gradually as time goes on. While, the irreversible fouling could be negligible all over the time, which indicates that hydraulic properties of NCM can be restored simply by backwashing. This conclusion is also supported

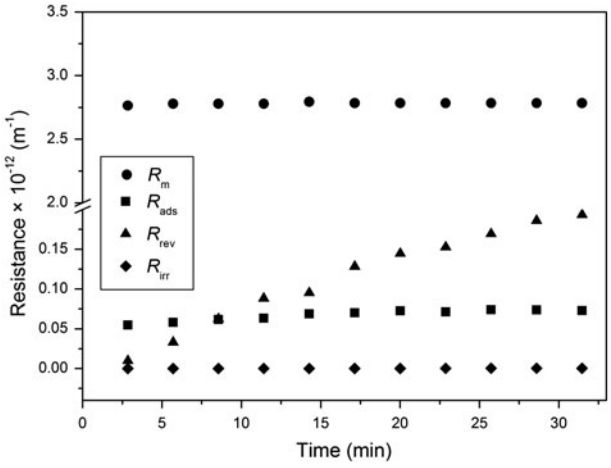

Fig. 11. Evolution of various resistances with time.

by the results of contact angle presented in Fig. 12, which is an indispensable tool in the respect of membrane fouling.

As can be seen in Fig. 12(a), the apparent contact angle on a fresh membrane is 15.1° implying a hydrophilic surface with an enhancement of antifouling ability. The metal cations contained in crystal lattices of the active layer can be hydrated in the presence of water. Therefore, a hydrophilic environment will appear on the surface of membrane [46]. The adsorbate on the surface or in membrane pores during filtration leads to the slightly fouling according to the static contact angle shown in Fig. 12(b). However, after backwashing, the hydrophilic property is restored with a contact angle of 15.8° labeled in Fig. 12(c). The small increase in contact angle indicates the inevitable solutes adsorbed on the membrane surface.

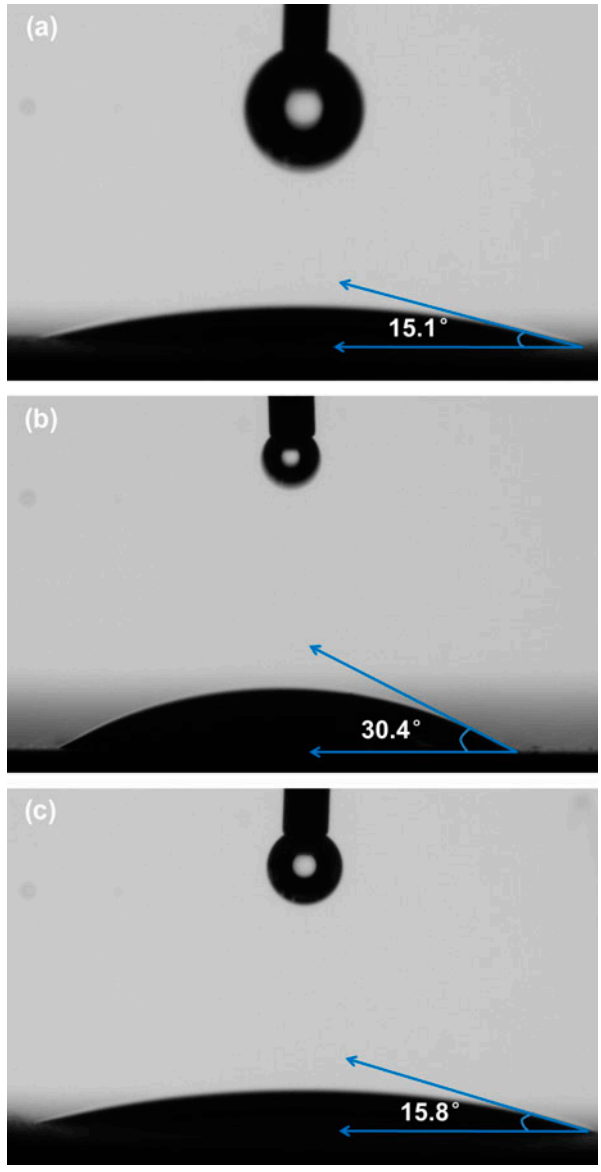

Fig. 12. Shape of the water droplets on (a) the new membrane, membrane (b) after filtration, and (c) membrane after backwashing (all the membranes were tested in dry state).

3.5. Influencing factors

Temperature and turbulence constitute main factors affecting the separation performance of membrane. In our study, the temperatures of feed solution were adjusted in the range from room temperature (~26℃)–57℃ via a thermel mounted in the experimental setup depicted in Fig. 1. Fig. 13(a) illustrates the variation of flux and salt concentration in the filtrate at different temperatures, which are all measured under the final steady state. As it can be observed, the permeability of NCM gradually meliorates with the increasing temperature accompanied by the substantial decrease of TSP concentration in the filtrate. Higher feed temperature leads to lower viscosity of the feed and also to weaken the intensity of the electroviscous effect in membrane pores. Consequently, the transport of solvent through the membrane intensifies, yielding a high permeate flux. High temperature can also reduce the concentration polarization, which enhances the diffusion of ions back toward the bulk solution. As a result, the solutes are largely retained by NCM. The other contribution to the lower TSP concentration in permeate side can be ascribed to the enhanced permeate flux, which may create the dilution effect for solutes in the filtrate [47].

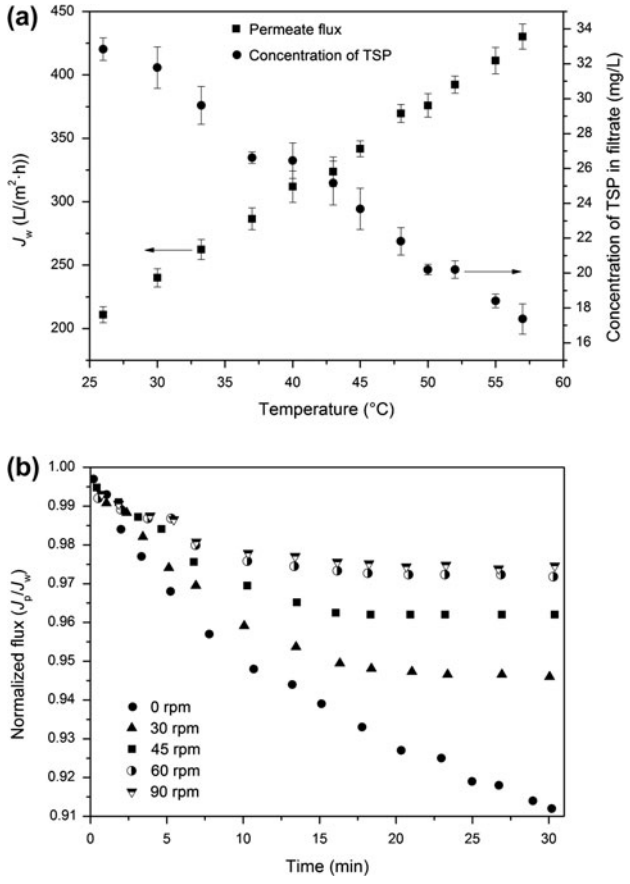

Fig. 13. Effect of (a) temperature and (b) stirring at room temperature on the permselectivity of NCM (initial concentration of TSP in the feed is 200 mg/L and driving pressure is 0.15 MPa).

Fig. 13(b) describes the influence of stirring on membrane permeability. Normalized flux is gradually recovered as the stirring speed increases. It is noteworthy that the permeate fluxes under stirring at 60 and 90 rpm vary in a similar manner, which indicates that the turbulence provided by stirring at 60 rpm has already disrupted concentration polarization layer sufficiently. Closer inspection of these data reveals that the permeability of NCM under strong turbulence (90 rpm) has not completely restored as that of the initial state. This result may be attributed to the deeply adsorbed species in membrane pores, which can cause adsorption resistance affecting the permeate flux negatively.

4. Conclusion

A nanoscale NCM has been prepared from the widespread natural clay through suspended powder technology. Packed clay flakes presented on the surface of membrane could not only hardly intrude into the pores of support, but also increase the tortuosity factor of active layer, which were conducive to improve the separation performance of NCM. XRF and FTIR results indicated that the raw clay might be the phyllosilicate. Similar components (SiO_2) made high compatibility and strong adhesion between the membrane and support. The transformation of crystal phase in active layer during sintering could provide a compact internal structure.

The performance of NCM was also investigated in the treatment of synthetic wastewater (TSP solutions). The results showed that NCM was capable of rejecting phosphate by electrostatic repulsion showing an IEP of pH around 6.4, which can result from amphoteric Al_2O_3 existing in the active layer. Therefore, relative high retention data for phosphate were obtained for the alkalinity of solution. In addition, the rejection rate decreased with the reduced decrement as the feed concentration increased, which could be attributed to the dilution effect and electroviscous phenomenon in membrane pores. Results also pointed to the membrane fouling mainly caused by concentration polarization, which could be significantly reduced through raising temperature and applying turbulence. The hydrophilicity could be restored by hydraulic washing without any harsh chemical cleaning.

The presented results might provide the rule of thumb for fabricating the membrane modules with other configurations (tubular or hollow fiber) in the successive studies. Allowing for the practical blowdown water from boilers, which is usually turbulent fluid with high temperature, it is an economic and efficient strategy to develop ceramic membrane from prevalent natural clay for water recycling in industries.

Acknowledgments

The authors acknowledge the financial support from National High-Tech Research Program of China (No. 2009AA03Z803) and Research Initiation Funds for Young Teachers of Beijing Technology and Business University (QNJJ2015-30).

Symbols

J	—	permeate flux
C_P	—	phosphate concentrations in the permeate
C_f	—	phosphate concentrations in the feed
ΔP	—	driving pressure
R_t	—	total filtration resistance
R_f	—	fouling resistance

R_m	—	membrane resistance
R_{ads}	—	adsorption resistance
R_{rev}	—	reversible fouling resistance
R_{irr}	—	irreversible fouling resistance

Greek

η	—	rejection rate
μ	—	dynamic viscosity

References

[1] M.B. Valcarce, M. Vázquez, Phosphate ions used as green inhibitor against copper corrosion in tap water, Corros. Sci. 52 (2010) 1413–1420.

[2] S. Mustafa, M.I. Zaman, S. Khan, Temperature effect on the mechanism of phosphate anions sorption by β-MnO_2, Chem. Eng. J. 141 (2008) 51–57.

[3] G. Wei, B.M. Fan, Y.P. Wei, S.S. Xu, Z.J. Zhao, N. Qiao, Preparation of a nano-scale ceramic membrane and its application in the medium-pressure boiler with phosphate treatment, Desalination 322 (2013) 167–175.

[4] X.L. Yuan, C.G. Bai, W.T. Xia, B. Xie, J. An, Phosphate adsorption characteristics of wasted low-grade iron ore with phosphorus used as natural adsorbent for aqueous solution, Desalin. Water Treat. 54 (2015) 3020–3030.

[5] S. Uludag-Demirer, M. Othman, Removal of ammonium and phosphate from the supernatant of anaerobically digested waste activated sludge by chemical precipitation, Bioresour. Technol. 100 (2009) 3236–3244.

[6] E. Salehi, S.S. Madaeni, A.A. Shamsabadi, S. Laki, Applicability of ceramic membrane filters in pretreatment of coke-contaminated petrochemical wastewater: Economic feasibility study, Ceram. Int. 40 (2014) 4805–4810.

[7] Q.H. Ng, J.K. Lim, A.L. Ahmad, B.S. Ooi, S.C. Low, Efficacy evaluation of the antifouling magnetite-PES composite membrane through QCM-D and magnetophoretic filtration performances, Sep. Purif. Technol. 132 (2014) 138–148.

[8] J. Luo, Y. Wan, Effects of pH and salt on nanofiltration—a critical review, J. Membr. Sci. 438 (2013) 18–28.

[9] M. Abbasi, M.R. Sebzari, S.R.H. Abadi, T. Mohammadi, T. Mahmood, Integrated membrane pilot plant for refinery wastewater treatment in order to produce boiler feedwater, Desalin. Water Treat. 51 (2013) 2543–2553.

[10] A.T.K. Tran, Y. Zhang, J. Lin, P. Mondal, W. Ye, B. Meesschaert, L. Pinoy, B. Van der Bruggen, Phosphate pre-concentration from municipal wastewater by selectrodialysis: Effect of competing components, Sep. Purif. Technol. 141 (2015) 38–47.

[11] R. Shang, A.R.D. Verliefde, J. Hu, Z. Zeng, J. Lu, A.J.B. Kemperman, H. Deng, K. Nijmeijer, S.G.J. Heijman, L.C. Rietveld, Tight ceramic UF membrane as RO pre-treatment: The role of electrostatic interactions on phosphate rejection, Water Res. 48 (2014) 498–507.

[12] J. Llanos, P.M. Williams, S. Cheng, D. Rogers, C. Wright, Á. Pérez, P. Cañizares, Characterization of a ceramic ultrafiltration membrane in different operational states after its use in a heavy-metal ion removal process, Water Res. 44 (2010) 3522–3530.

[13] A. Majouli, S. Tahiri, S. Alami Younssi, H. Loukili, A. Albizane, Elaboration of new tubular ceramic membrane from local Moroccan Perlite for microfiltration process. Application to treatment of industrial wastewaters, Ceram. Int. 38 (2012) 4295–4303.

[14] I.N. Widiasa, A.A. Susanto, H. Susanto, Performance of an integrated membrane pilot plant for wastewater reuse: case study of oil refinery plant in Indonesia, Desalin. Water Treat. 52 (2014) 7443–7449.

[15] F.A. Jumeri, H.N. Lim, S.N. Ariffin, N.M. Huang, P.S. Teo, S.O. Fatin, C.H. Chia, I. Harrison, Microwave synthesis of magnetically separable $ZnFe_2O_4$-reduced graphene oxide for wastewater treatment, Ceram. Int. 40 (2014) 7057–7065.

[16] M.G. Buonomenna, Membrane processes for a sustainable industrial growth, RSC Adv. 3 (2013) 5694–5740.

[17] J. Xu, C.Y. Chang, C. Gao, Performance of a ceramic ultrafiltration membrane system in pretreatment to seawater desalination, Sep. Purif. Technol. 75 (2010) 165–173.

[18] Q. Chang, J.-E. Zhou, Y. Wang, J. Liang, X. Zhang, S. Cerneaux, X. Wang, Z. Zhu, Y. Dong, Application of ceramic microfiltration membrane modified by nano-TiO_2 coating in separation of a stable oil-in-water emulsion, J. Membr. Sci. 456 (2014) 128–133.

[19] J.-E. Zhou, Q. Chang, Y. Wang, J. Wang, G. Meng, Separation of stable oil-water emulsion by the hydrophilic nano-sized ZrO_2 modified Al_2O_3 microfiltration membrane, Sep. Purif. Technol. 75 (2010) 243–248.

[20] Y. Wang, H. Liu, H. Cheng, J. Wang, Fabrication and properties of 3D oxide fiber-reinforced Al_2O_3-SiO_2-SiOC composites by a hybrid technique based on sol-gel and PIP process, Ceram. Int. 41 (2015) 1065–1071.

[21] E. Zuriaga-Agustí, E. Alventosa-deLara, S. Barredo-Damas, M.I. Alcaina-Miranda, M.I. Iborra-Clar, J.A. Mendoza-Roca, Performance of ceramic ultrafiltration membranes and fouling behavior of a dye-polysaccharide binary system, Water Res. 54 (2014) 199–210.

[22] S. Muthukumaran, K. Baskaran, Comparison of the performance of ceramic microfiltration and ultrafiltration membranes in the reclamation and reuse of secondary wastewater, Desalin. Water Treat. 52 (2014) 670–677.

[23] K. Rodemann, E. Staude, Electrokinetic characterization of porous membranes made from epoxidized polysulfone, J. Membr. Sci. 104 (1995) 147–155.

[24] E. Nowak, P. Robbins, G. Combes, E.H. Stitt, A.W. Pacek, Measurements of contact angle between fine, non-porous particles with varying hydrophobicity and water and non-polar liquids of different viscosities, Powder Technol. 250 (2013) 21–32.

[25] M.D. Hurtado, S. Carmona, A. Delgado, Automated modification of the molybdenum blue colorimetric method for phosphorus determination in soil extracts, Commun. Soil Sci. Plant Anal. 39 (2008) 2250–2257.

[26] S.J. Lee, J.-H. Kim, Differential natural organic matter fouling of ceramic versus polymeric ultrafiltration membranes, Water Res. 48 (2014) 43–51.

[27] A. Urbanowska, M. Kabsch-Korbutowicz, Influence of operating conditions on performance of ceramic membrane used for water treatment, Chem. Pap. 68 (2014) 190–196.

[28] V.M.M. Lobo, Handbook of Electrolyte Solutions: Part A and Part B, Elsevier, Amsterdan, 1989.
[29] L.G. Baikova, R.I. Mamalimov, T.I. Pesina, A.E. Chmel, A.I. Shcherbakov, Structural Transformations During Heat-Treatment of Quartz Ceramic, Glass Ceram. 70 (2013) 303–305.
[30] J. Schaep, C. Vandecasteele, B. Peeters, J. Luyten, C. Dotremont, D. Roels, Characteristics and retention properties of a mesoporous γ-Al_2O_3 membrane for nanofiltration, J. Membr. Sci. 163 (1999) 229–237.
[31] Y.L. Elaine Fung, H. Wang, Investigation of reinforcement of porous alumina by nickel aluminate spinel for its use as ceramic membrane, J. Membr. Sci. 444 (2013) 252–258.
[32] L.F. Han, Z.L. Xu, Y. Cao, Y.M. Wei, H.T. Xu, Preparation, characterization and permeation property of Al_2O_3, Al_2O_3–SiO_2 and Al_2O_3–kaolin hollow fiber membranes, J. Membr. Sci. 372 (2011) 154–164.
[33] H.M. Zhou, X.C. Qiao, J.G. Yu, Influences of quartz and muscovite on the formation of mullite from kaolinite, Appl. Clay Sci. 80–81 (2013) 176–181.
[34] P. Yuan, D. Tan, F. Aannabi-Bergaya, W. Yan, M. Fan, D. Liu, H. He, Changes in structure, morphology, porosity, and surface activity of mesoporous halloysite nanotubes under heating, Clays Clay Miner. 60 (2012) 561–573.
[35] S.W. Yung, H.Y. Chiang, Y.S. Lai, F.B. Wu, C. Fu, Y.M. Lee, Thermal, optical and structural properties of Tb doped zinc aluminum phosphate glasses, Ceram. Int. 41 (2015) 877–888.
[36] S. Yariv, I. Lapides, A. Nasser, N. Lahav, I. Brodsky, K.H. Michaelian, Infrared Study of the intercalation of potassium halides in kaolinite, Clays Clay Miner. 48 (2000) 10–18.
[37] K.W. Ryu, Y.N. Jang, S.C. Chae, Hydrothermal synthesis of kaolinite and its formation mechanism, Clays Clay Miner. 58 (2010) 44–51.
[38] S.A.M. den Hartog, D.M. Saffer, C.J. Spiers, The roles of quartz and water in controlling unstable slip in phyllosilicate-rich megathrust fault gouges, Earth Planets Space 66 (2014) 78–86.
[39] M. Abbasi, D. Mowla, Analysis of membrane pore-blocking models applied to the MF of real oily wastewaters treatment using mullite and mullite-alumina ceramic membranes, Desalin. Water Treat. 52 (2014) 2481–2493.
[40] S.M.S. Shahabadi, A. Reyhani, Optimization of operating conditions in ultrafiltration process for produced water treatment via the full factorial design methodology, Sep. Purif. Technol. 132 (2014) 50–61.
[41] J. Kaewsuk, D.Y. Lee, T.S. Lee, G.T. Seo, Effect of ion composition on nanofiltration rejection for desalination pretreatment, Desalin. Water Treat. 43 (2012) 260–266.
[42] W.R. Bowen, H.N.S. Yousef, Effect of salts on water viscosity in narrow membrane pores, J. Colloid Interface Sci. 264 (2003) 452–457.
[43] B. Tansel, J. Sager, T. Rector, J. Garland, R.F. Strayer, L. Levine, M. Roberts, M. Hummerick, J. Bauer, Significance of hydrated radius and hydration shells on ionic permeability during nanofiltration in dead end and cross flow modes, Sep. Purif. Technol. 51 (2006) 40–47.
[44] C. Mazzoni, L. Bruni, S. Bandini, Nanofiltration: Role of the electrolyte and pH on desal DK performances †, Ind. Eng. Chem. Res. 46 (2007) 2254–2262.
[45] R. Valladares Linares, Z. Li, S. Sarp, S.S. Bucs, G. Amy, J.S. Vrouwenvelder, Forward osmosis niches in seawater desalination and wastewater reuse, Water Res. 66 (2014) 122–139.
[46] Z.B. Ouznadji, M.N. Sahmoune, N.Y. Mezenner, Adsorptive removal of diazinon: kinetic and equilibrium study, Desalin. Water Treat. (2014) 1–10.
[47] S. Muthukumaran, J.V. Jegatheesan, K. Baskaran, Comparison of fouling mechanisms in low-pressure membrane (MF/UF) filtration of secondary effluent, Desalin. Water Treat. 52 (2014) 650–662.